J. metamorphic Geol., 2009, **27,** 757–772 doi:10.1111/j.1525-1314.2009.00831.x

Metamorphic *P–T* conditions and thermal structure of Chinese Continental Scientific Drilling main hole eclogites: Fe–Mg partitioning thermometer *vs.* Zr-in-rutile thermometer

R. Y. ZHANG,[1] Y. IIZUKA,[2] W. G. ERNST,[1] J. G. LIOU,[1] Z.-Q. XU,[3] T. TSUJIMORI,[4] C.-H. LO[5] AND B.-M. JAHN[2]

[1]*Department of Geological & Environmental Sciences, Stanford University, Stanford, 94305-2115 CA, USA (ry.zhang@stanford.edu)*

[2]*Institute of Earth Sciences, Academia Sinica, Nankang, 11529 Taipei, Taiwan*

[3]*Institute of Geology, Chinese Academy of Geological Sciences, 100037 Beijing, China*

[4]*Institute for Study of the Earth Interior, Okayama University, Misasa, 682-0193 Tottori, Japan*

[5]*Department of Geosciences, National Taiwan University, 106 Taipei, Taiwan*

ABSTRACT Core rocks recovered from the main hole (5158 m deep) of the Chinese Continental Scientific Drilling (CCSD-MH) project, southern Sulu UHP terrane, east-central China, consist of eclogites, various gneisses and minor metaperidotite cumulates; this lithological section underwent subduction-zone UHP metamorphism. Coesite-bearing eclogites are mainly present between the depths of 100–2000 m, but below 2000 m, mafic eclogites are rare. Selected elements (Zr, Nb, Cr, Fe, Si, Mg, Al & Ti) in rutile from 39 eclogite cores from 100 to 2774 m, and major elements of minerals from representative eclogites were analysed by electron microprobe. Zirconium and Nb concentrations of rutile cluster ~100–400 and 200–700 ppm respectively. However, Zr and Nb contents in rutile from strongly retrograded eclogites show larger variations than those of fresh or less retrograded eclogites, implying that somehow fluid infiltration affected rutile chemistry during retrograde metamorphism. Zr contents in rutile inclusions in garnet and omphacite are slightly lower than those of the matrix rutile, suggesting that the rutile inclusions formed before or close to the peak temperature. The *P–T* conditions of the CCSD-MH eclogites were estimated by both Fe–Mg exchange and Zr-in-rutile thermometers, as well as by the Grt–Cpx–Phn–Ky geothermobarometer. The maximum temperature range of 700–811 °C calculated at 40 kbar using the Zr-in-rutile thermometer is comparable with temperature estimates by the Fe–Mg exchange thermometer. The temperature estimates of eclogites in a ~3000 m thick section define a continuous gradient, and do not show a distinct temperature gap, suggesting that the rocks from 100 to 3000 m depth might belong to a single, large-scale UHP slab. These data combined with *P–T* calculations for CCSD-MH peridotites yield a low geotherm (~5 °C km^{-1}) for the Triassic subduction zone between the Sino-Korean and Yangtze cratons; it lies ~30–35 mW m^{-2} conductive model geotherm.

Key words: Chinese Continental Scientific Drilling; Fe–Mg exchange thermometer; Sulu UHP eclogite; thermal structure; Zr-in-rutile thermometer.

INTRODUCTION

The main hole (MH) of the Chinese Continental Scientific Drilling (CCSD) project at Donghai, southern Sulu UHP terrane, east-central China reveals a continuous lithological profile 5158 m thick, which consists of interlayered UHP gneisses, eclogites and minor peridotites. The total thickness of eclogite is ~1030 m between the depths of 100–3000 m; this section provides a unique opportunity to determine the fossil thermal structure of the Triassic Sulu subduction zone juxtaposing the Sino-Korean and Yangtze cratons. Conventionally, Fe–Mg partitioning thermometers such as Grt–Cpx and thermobarometers such as Grt–Cpx–Phn–Ky (mineral symbols after Kretz, 1983) allow the estimation of metamorphic *P–T* conditions for eclogites. Rutile is the most common minor mineral and represents a major carrier of high-field strength elements in eclogites. The solubility of ZrO_2 in rutile is strongly temperature-dependent, therefore, the Zr content of rutile in the quartz + zircon-bearing system has been developed as a potential thermometer over the last several years (Zack *et al.*, 2004; Watson *et al.*, 2006). More recently, experimental study in the ZrO_2–TiO_2–SiO_2 system at 1 atm, and at 10, 20 and 30 kbar, and temperatures between 1000 and 1500 °C suggests that the Zr content of rutile decreases with increasing pressure; thus a new Zr-in-rutile thermometer has been

produced (Tomkins *et al.*, 2007). Moreover, the Ti-in-zircon and Zr-in-rutile thermometers not only consider Zr abundance in rutile, but also involve the activities of SiO_2 and TiO_2; the zircon thermometer may now be applied to rocks without quartz and/or rutile, and the rutile thermometer might be used for rocks without quartz in cases where the activities of SiO_2 and TiO_2 can be estimated (Ferry & Watson, 2007).

In the present study, a large number of analyses of rutile (including Si, Al, Mg, Fe, Zr, Nb) are provided from 39 representative eclogite cores from the 101 to 2774 m depth range. Major element data on minerals are also presented from selected representative eclogites. Fe–Mg exchange and Zr-in-rutile thermometers, and the Grt–Cpx–Phn–Ky geothermobarometer are applied to estimate metamorphic *P–T* conditions of these rocks. These new results, combined with previously published *P–T* data for both CCSD-MH eclogites and peridotites are used to reconstruct the thermal structure of the Triassic Sulu subduction zone between the Sino-Korean and the Yangtze cratons.

CCSD-MH IN THE SULU UHP TERRANE

The Sulu terrane is the eastern extension of the well-documented Triassic continent–continent collision zone between the Sino-Korean and Yangtze cratons (Fig. 1). The terrane is made up of a fault-bounded UHP coesite-bearing eclogite belt on the north-west, and a HP belt consisting of quartz–mica schist, chloritoid–kyanite–mica–quartz schist, marble and rare blueschist on the south-east (Zhang *et al.*, 1995). The MH drill site of the CCSD is in the Donghai area, southern Sulu UHP belt. Here, abundant eclogite lenses and layers are interstratified with gneiss and marble and peridotites occur as blocks in gneiss and as layers in eclogite. Coesite inclusions occur in eclogitic minerals and in zircon crystals, which are present in both eclogitic and gneissic rocks. The supracrustal and mafic-ultramafic rocks were subjected to Triassic (240–220 Ma) (Jahn *et al.*, 2003; Yang *et al.*, 2003; Hacker *et al.*, 2004; Liu *et al.*, 2004, 2006, 2008; Liu & Xu, 2005; Zhang *et al.*, 2005a; Zheng *et al.*, 2006; Chen *et al.*, 2007) *in situ* subduction-zone UHP metamorphism at 750–950 °C and 4–6.5 GPa (Liu *et al.*, 2006; Yang & Jahn, 2000; Zhang *et al.*, 1995, 2000, 2003, 2005b, 2008; Zhang *et al.*, 2006b), followed by a granulite- to amphibolite facies retrograde overprint.

Lithology and ages of the CCSD-MainHole

UHP rocks recovered from the CCSD-MH include eclogites, various gneisses and minor ultramafic rocks. Eclogites with gneissic interlayers mainly occur in the intervals 100–1100 and 1600–2038 m; only thin layers or minor lenses, such as at 2675–2775 m (Fig. 2) are

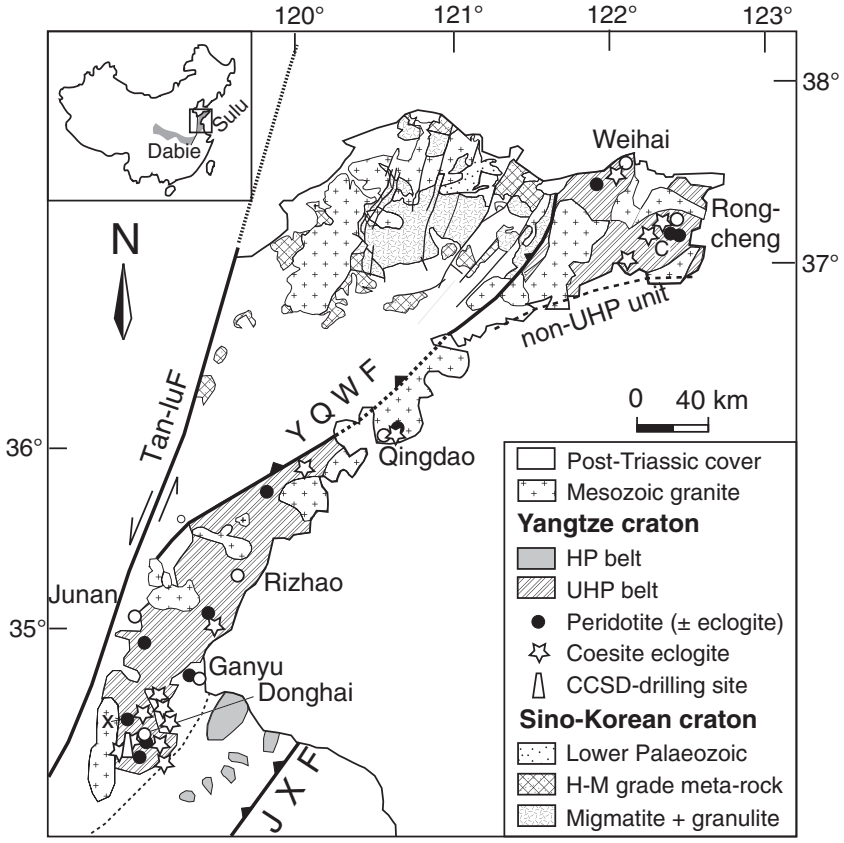

Fig. 1. Geological sketch map of the Sulu UHP terrane showing drill site of the Chinese Continental Scientific Drilling project. YQWF, Yantai-Qingdao-Wulian fault; JXF, Jianshan-Xiangshui fault (modified after Zhang *et al.*, 2009).

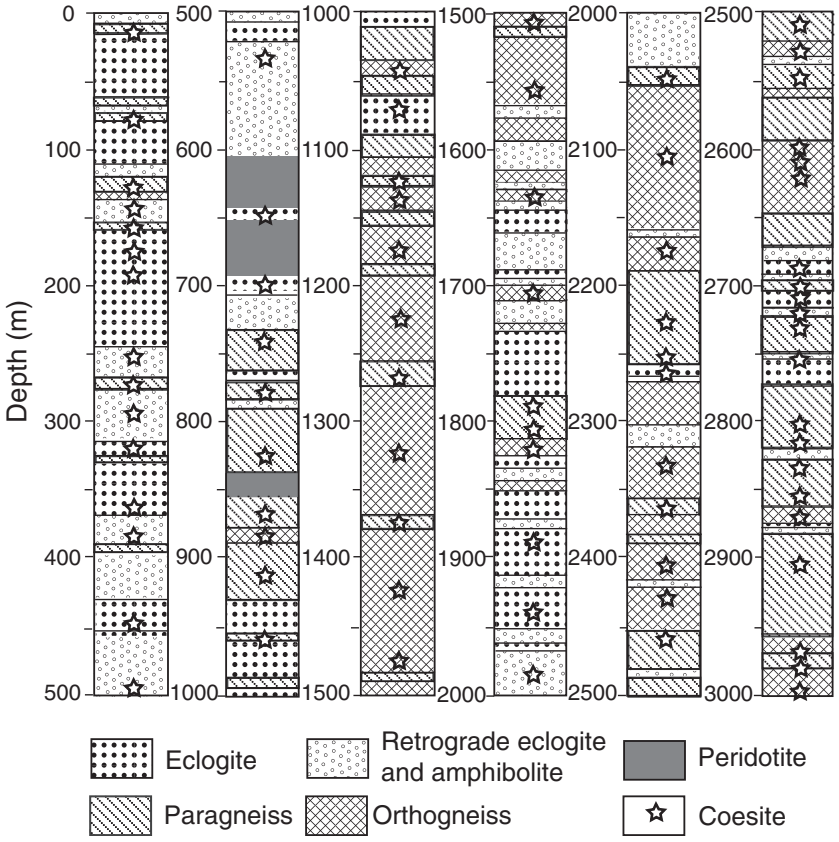

Fig. 2. Lithological profile of CCSD main hole modified after Liu *et al.* (2007).

present deeper than 2038 m. Inclusions of coesite or quartz pseudomorphs after coesite were identified in eclogitic garnet and omphacite, and in zircon of all rock types from the surface to 5158 m depth (Liu *et al.*, 2007). From 0 to 100 m, only rock cuttings were collected. Assemblages of the CCSD-MH from 100 to 3000 m were divided into seven units according to rock associations and bulk compositions. Unit 1 (100–530 m) is mainly composed of phengite-bearing, quartz-rich eclogites with minor rutile-rich eclogite and paragneiss. Unit 2 (530–600 m) consists of quartz-free, rutile-rich eclogites and ilmenite-rich garnet clinopyroxenite. Unit 3 (600–680 m) comprises garnet wehrlite, websterite, clino- and orthopyroxenites, including a single thin layer of eclogite. Unit 4 (680–1160 m) is composed of paragneiss, eclogite, amphibolite and a thin lens of serpentinite at 843–851 m. Unit 5 (1160–1600 m) consists of orthogneiss, paragneiss and amphibolite. Unit 6 (1600–2190 m) is made up mainly of eclogite and paragneiss (modified after Zhang *et al.*, 2006c). Most amphibolites are completely retrograde eclogites. Paragneiss and orthogneiss are the major constitutions in deep part of MH, 2190–3000 m (unit 7); eclogite is minor.

SHRIMP U–Pb analyses of zircon grains from CCSD-MH eclogites yield ages of 784–774 Ma for magmatic cores and 229–221 Ma for UHP metamorphic domains (Chen *et al.*, 2007; Zhang *et al.*, 2006b; Liu *et al.*, 2008). Some slightly younger zircon rim ages 218–216 Ma reported by Zhang *et al.* (2006b) might reflect the retrograde metamorphic overprint.

Eclogite petrography

Except for a few bimineral eclogites, all recovered eclogitic cores contain coesite/quartz (Fig. 3a), rutile and accessory zircon and apatite. Based on mineral paragenesis, the eclogites can be simply classified as (i) phengite-bearing eclogites; (ii) quartz-free eclogites (such as B352, a wall rock of the ultramafic rocks); (iii) quartz-rich eclogites; (iv) rutile-rich eclogites and (v) kyanite ($\pm$phengite $\pm$ zoisite)-bearing eclogites (e.g. B555, B589, B1015). Jadeite occurs in some phengite-bearing eclogites (e.g. B88). Ilmenite, as a major Ti-bearing phase, is present in a few garnet clinopyroxenites (such as B278) that have been described as eclogite (Zhang *et al.*, 2006b). Eclogites (ii), (iii) and (v) do not show a distinct difference from phengite-bearing eclogite in texture. The petrography of phengite-bearing and kyanite-bearing eclogites is briefly described below.

Phengite eclogite (Grt + Omp + Qtz + Phn) is the most abundant type of eclogite (>90%) in the CCSD-MH, and phengite or quartz contents in some eclogites range up to >10 vol%. Most phengite-bearing eclogites are massive, showing granoblastic

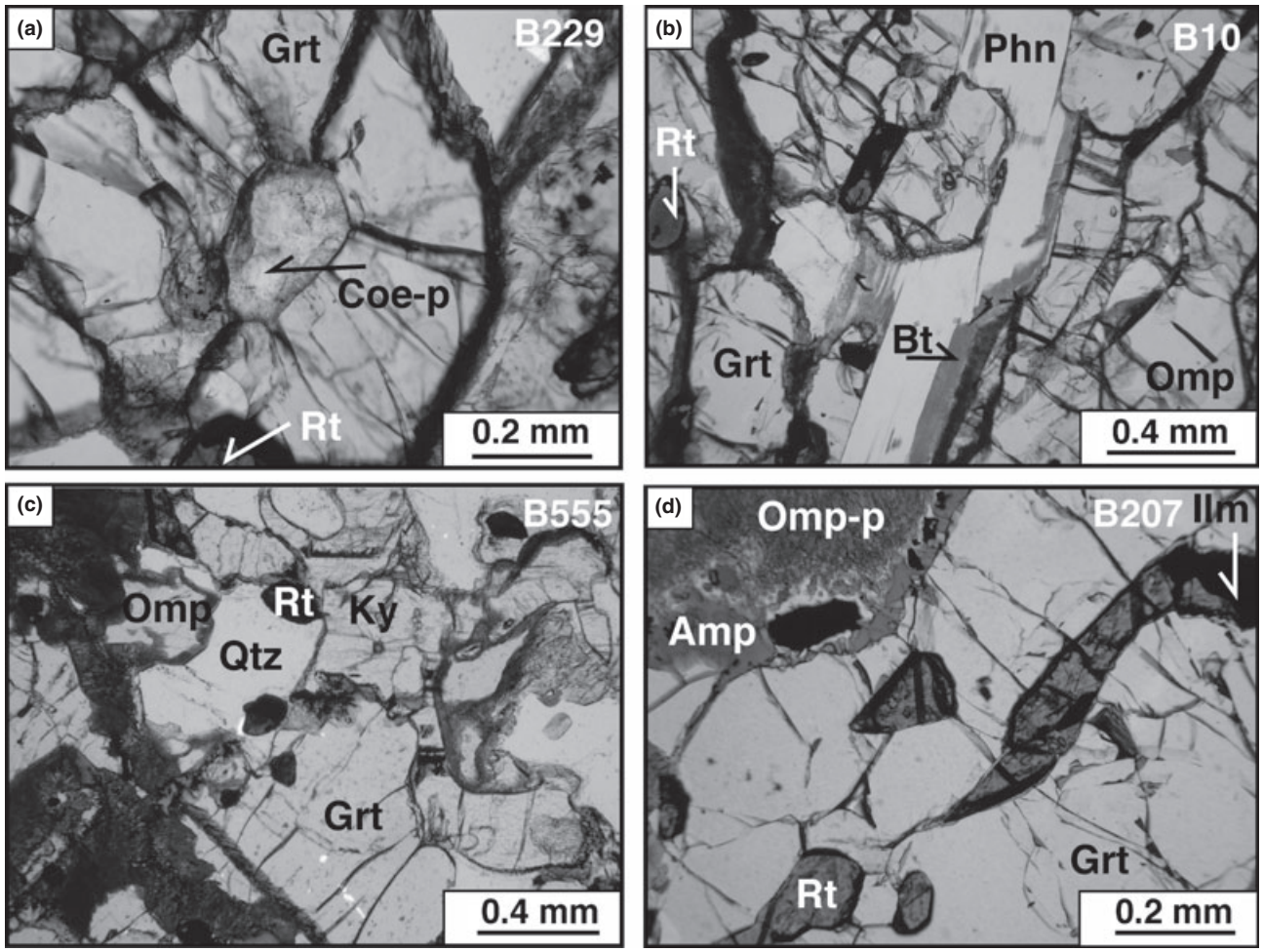

Fig. 3. Photomicrographs showing mineral parageneses and textures of eclogites: (a) quartz pseudomorph after coesite in garnet (B229); (b) Phn-bearing eclogite (B10); (c) Ky-bearing eclogite (B555) and (d) Rt-rich eclogite (B207). Omp-p, symplectite after omphacite; Coe-p, quartz pseudomorph after coesite. All photomicrographs are in plane polarized light.

texture; foliated phengite-bearing eclogite is uncommon. Garnet and omphacite display a range in grain size from 0.5 to 3 mm. Minerals exhibit retrograde alteration: garnet is rimed by amphibole, omphacite is replaced by Amp + Pl ± Cpx with low jadeite content and phengite is overprinted by very fine-grained biotite along its margins (Fig. 3b).

Kyanite-bearing eclogites with granoblastic texture include three assemblages: Grt + Omp + Coe/Qtz + Ky + Phn (B555), Grt + Omp + Coe/Qtz + Ky + Zo (B589) and Grt + Omp + Coe/Qtz + Ky + Phn + Zo (B1015). Eclogites B555 and B589 are quartz-rich, but B1015 contains only minor quartz. Garnet and omphacite are 0.5–3 mm in size (Fig. 3c). Rounded garnet contains inclusions of quartz, zoisite, amphibole, omphacite and rutile. Omphacite is rimed by very fine-grained symplectite. Kyanite ($< 5\%$) contains inclusions of quartz and garnet, partially rimed by fine-grained albite. Foliated kyanite-bearing eclogite (sample B1015) shows a porpyroblastic texture. Coarse-grained (1–3.5 mm) zoisite (5–10% vol%) with a poikiloblastic texture is set in a matrix of fine-grained garnet (0.15–0.6 mm in size) and relative coarser omphacite, kyanite and orientated phengite and contain numerous inclusions of garnet, omphacite, quartz and rutile.

ANALYTICAL METHODS

Major elements of eclogitic minerals

Major elements of minerals were analysed employing a JEOL superprobe 733 equipped with five spectrometers operating as a wavelength dispersive system (WDS) at Stanford University, and a JEOL electron probe micro-analyser (EPMA) JXA-8900R at the Institute of Earth Sciences, Academia Sinica, Taiwan. At Stanford University, the analysed standards were Amelia albite for Na, San Carlos olivine for Mg, spessartine (Pala CA.) for Al and Mn, wollastonite for

Si and Ca, orthoclase (Stanford collection) for K, synthetic rutile for Ti, Australian chromite for Cr and New York hematite for Fe. Operating conditions were 15 kV and 20 nA beam current. The electron beam size was ~0.5 μm; the X-ray beam diameter was ~2 μm; the counting time was 20 s. Analysed precision depends on elemental content: ±1% for wt% >7–10% elements, better than 2% for most elements except Na (2–3%) and from ±10% to ±50% for minor and trace elements respectively. Operating conditions of the electron probe JXA-8900R were similar to those used for the superprobe 733.

Trace elements of rutile

The elements Ti, Zr, Nb, Al, Fe, Cr, Mg and Si in rutile were analysed using the Institute of Earth Sciences, Academia Sinica JEOL EPMA. The EPMA was equipped with four WDS with beam current of 200 nA and a focused beam at an acceleration voltage of 20 kV. Analyses were corrected by the metal PRZ method (Reed, 1993) using calibration of synthetic chemically known standards with various counting times and diffracting crystals: Zr- and Nb-free rutile for Ti-Kα (15 and 5 s: for peak, and both upper and lower baselines with PET crystal) and O-Kα (30 and 10 s with LED1H crystal), Ti- and Nb-free zircon for Zr-Lα (200 and 30 s with PETH crystal), lithium niobate ($LiNbO_3$) for Nb-Lα (200 and 30 s with PETH crystal), hematite for Fe-Kα (100 and 20 s with LIFH crystal) and chromium oxide (Cr_2O_3) for Cr-Kα (150 s and 30 s with PET crystal). Detailed conditions for the analyses are shown in Table 1. To assess elemental contamination from surrounding, mostly silicate minerals, Si-Kα and Al-Kα were also measured during rutile analysis. Quantitative analyses for Zr and Nb with EPMA were confirmed by chemically known rutile with 98–769 ppm Zr and 145–2592 ppm Nb, respectively, measured by ICP-MS (T. Zack, Pers. comm.); correlation coefficients between the ICP-MS and the WDS-EPMA of $r^2 = 0.991$ for Zr and 0.996 for Nb were obtained. Detection limit based on 3σ of standard calibration were ~30 ppm for Zr and Nb, and ~10 ppm for Fe and Cr.

MINERAL COMPOSITIONS OF THE CCSD-MH ECLOGITES

Major minerals

Fresh and less alterative eclogites preserve the peak metamorphic assemblage of Grt + Omp + Coe + Phn ± Ky. In a few eclogites, zoisite was also stable under the UHP conditions. Secondary minerals include amphibole, plagioclase, biotite and epidote and ilmenite after rutile. Representative mineral compositions are listed in Table 2, although there are numerous analyses for individual phases (some more than 20 point analyses).

Garnet is relatively homogenous in a single rock sample, but varies from layer to layer. It displays large variations in almandine and pyrope components, whereas in contrast, the grossular component shows a small range ($alm_{25\text{-}60}prp_{14\text{-}48}grs_{15\text{-}29}sps_{00\text{-}02}$, Fig. 4). This mainly depends on the bulk composition of an eclogite at a given *P–T* condition. The prp component decreases with increasing alm component; sps in all garnet grains is low (most <2 mole%).

Omphacite of the studied eclogites exhibits significantly variation in jadeite and aegirine components (Fig. 5) ranging from 34 to 70 mole% and 0–16 mole% (Fe^{3+} = Na–Al) respectively. The Na_2O contents of omphacite show a pronounced positive correction with Al_2O_3 (Table 2). Retrograde Cpx crystals in symplectites are aegirine–augite (Aeg) or Cpx on the boundary between omphacite and augite with low jadeite component (21 mole%).

Phengite is widespread in the CCSD-MH eclogites, and is characterized by high Si values (3.45–3.68 pfu); phengite having Si <3.5 pfu might be attributed to retrograded metamorphism. Zoisite grains with X_{Fe} [$Fe^{3+}/(Al + Fe^{3+})$] between 0.04 and 0.05 (total Fe express as Fe^{3+}) are present in kyanite-bearing eclogites. Amphibole and albite are the most common secondary minerals.

Minor minerals – rutile

Rutile is present in all eclogites, occurring as fine-grained inclusions in garnet and omphacite, or as a

Table 1. Conditions of electron microprobe for rutile trace element analysis.

Channel	1			2		3			4
Element Standard	Al-Kα Corundum	Si-Kα Zircon	Mg-Kα Periclase	O-Kα Rutile	Nb-Lα LiNbO3	Zr-Lα Zircon	Fe-Kα Hematite	Ti-Kα rutile	Cr-Kα Cr_2O_3
WDS setting									
Diffracting crystal	TAP	TAP	TAP	LED1H	PETH	PETJ	LIFH	PETJ	PETJ
Peak (mm)	90.5	77.2	107.5	110.0	183.4	194.4	134.5	88.1	73.3
Baseline (+, mm)	5	3.4	5	9.5	6.5	7.6	3	5	4.5
Baseline (–, mm)	7	4.7	8	6	5.0	4.5	5.5	4.5	4.5
Count peak (s)	200	30	150	30	200	200	100	15	150
Counts baseline (s)	30	10	30	10	30	30	20	5	30
Exposure time (s)	260	50	210	50	260	260	140	25	210

Primary beam conditions: focused beam at acceleration voltage of 20 kV; beam current at 200 nA. Total beam exposure time for each analysis: 660 s.

Table 2. Mineral compositions of CCSD-MH eclogites.

(a)

Sample	B1R (Zhang *et al.*, 2006b)			B10			B36			B136		B146	
mineral	Grt	Omp	Phn	Grt	Omp	Phn	Grt	Omp	Phn	Grt	Omp	Grt	Omp
SiO_2	38.19	57.22	52.07	38.74	58.40	53.22	39.50	56.10	54.66	39.62	56.81	38.14	56.04
TiO_2	0.03	0.05	0.45	0.08	0.08	0.48	0.00	0.11	0.38	0.01	0.06	0.00	0.00
Cr_2O_3	0	0.02	0.04	0	0.00	0.00	0.02	0.15	0.00	0.00	0.03	0.00	0.00
Al_2O_3	21.45	16.28	23.40	21.47	16.80	23.03	22.19	10.59	21.60	22.24	11.93	21.52	7.95
FeO	26.59	5.26	2.99	25.79	4.68	2.85	21.64	4.12	1.76	25.64	5.70	26.96	7.62
MnO	1.08	0.05	0.03	1.09	0.00	0.08	0.66	0.01	0.04	0.54	0.00	0.66	0.00
MgO	3.69	3.9	4.15	3.96	3.38	4.05	9.29	8.04	5.49	6.50	7.05	6.35	8.21
CaO	9.51	6.41	0	10.04	6.00	0.00	6.29	12.30	0.04	8.05	10.90	5.37	12.44
Na_2O	0.06	10.7	0.28	0.03	11.44	0.29	0.01	7.03	0.12	0.06	7.84	0.00	6.63
K_2O			10.66	0.00	0.02	10.49	0.00	0.00	10.57	0.00	0.00	0.00	0.00
Total	100.60	99.89	94.07	101.20	100.80	94.49	99.60	98.45	94.66	102.66	100.34	99.01	98.91
Si	2.990	2.010	3.535	3.004	2.024	3.584	3.009	2.019	3.651	2.993	2.012	2.998	2.044
Ti	0.002	0.001	0.023	0.005	0.002	0.025	0.000	0.003	0.019	0.000	0.002	0.000	0.000
Cr	0.000	0.001	0.002	0.000	0.000	0.000	0.001	0.004	0.000	0.000	0.001	0.000	0.000
Al	1.980	0.674	1.873	1.963	0.686	1.828	1.993	0.449	1.701	1.980	0.498	1.994	0.342
Fe^{3+}		0.055			0.083			0.042			0.040		0.127
Fe^{2+}	1.741	0.100	0.170	1.673	0.053	0.161	1.379	0.082	0.098	1.620	0.129	1.773	0.105
Mn	0.072	0.001	0.002	0.071	0.000	0.004	0.042	0.000	0.002	0.035	0.000	0.044	0.000
Mg	0.431	0.204	0.420	0.458	0.175	0.407	1.055	0.431	0.547	0.731	0.372	0.745	0.446
Ca	0.798	0.241	0.000	0.834	0.223	0.000	0.513	0.474	0.003	0.652	0.414	0.452	0.486
Na	0.009	0.729	0.037	0.005	0.769	0.038	0.002	0.491	0.016	0.009	0.538	0.000	0.469
K	0.000	0.000	0.923	0.000	0.001	0.901	0.000	0.000	0.901	0.000	0.000	0.000	0.000
Total	8.023	4.016	6.985	8.012	4.015	6.947	7.995	3.996	6.938	8.020	4.006	8.005	4.020
$1X_{Fe^{3+}}$		0.355			0.608			0.339			0.237		0.547
$2X_{Fe^{3+}}$	0.039	0.309		0.022	0.340		0	0		0.038	0.106	0.009	0.255
K_{D1}	8.256			12.007			6.875			6.391		10.124	
K_{D2}	7.435			6.968			4.546			5.247		6.082	

(b)

	B244				B352				B555			B589	
	Grt	Omp	Phn	Rt	Ilm	Grt	Omp	Grt	Omp	Ky	Phn	Grt	Omp
SiO_2	38.03	55.38	54.25	0.04	0.01	40.80	57.15	39.90	56.77	37.22	52.42	41.64	56.74
TiO_2	0.00	0.14	0.63	100.48	53.88	0.01	0.08	0.07	0.05	0.03	0.28	0.04	0.05
Cr_2O_3	0.02	0.08	0.02	0.10	0.00	0.01	0.00	0.00	0.00	0.00	0.00	0.00	0.05
Al_2O_3	21.15	9.36	20.76	0.08	0.03	23.12	11.76	21.40	10.74	60.22	23.22	23.07	8.07
FeO[a]	29.95	8.88	2.80	0.41	43.14	17.44	2.41	21.18	7.94	1.67	2.96	12.43	1.38
MnO	0.81	0.08	0.02	0.06	0.22	0.42	0.00	0.50	0.00	0.02	0.03	0.27	0.00
MgO	4.53	6.36	4.90	0.01	2.26	11.96	8.68	9.87	6.54	0.02	4.13	13.67	11.88
CaO	5.92	11.47	0.10	0.05	0.14	7.34	12.97	7.45	9.90	0.00	0.04	10.37	16.74
Na_2O	0.02	7.45	0.42	0.01	0.01	0.00	6.92	0.01	8.88	0.00	0.44	0.02	4.74
K_2O	0.00	0.00	8.92	0.00	0.00	0.00	0.02	0.00	0.02	0.01	9.73	0.00	0.02
Total	0.000	99.19	92.81	101.24	99.69	101.10	100.01	100.38	100.84	99.19	93.25	101.51	99.67
Si	2.996	2.025	3.683	0.000	0.000	3.001	2.008	3.019	2.025	1.016	3.567	3.005	2.011
Ti	0.000	0.004	0.032	0.994	1.005	0.001	0.002	0.004	0.001	0.001	0.015	0.002	0.001
Cr	0.001	0.002	0.001	0.001	0.000	0.001	0.000	0.000	0.000	0.000	0.000	0.000	0.001
Al	1.964	0.403	1.661	0.001	0.001	2.005	0.487	1.909	0.451	1.938	1.862	1.963	0.337
Fe^{3+}		0.125		0.000	0.000		0.000		0.163				
Fe^{2+}	1.973	0.147	0.159	0.005	0.895	1.073	0.071	1.340	0.074	0.038	0.168	0.750	0.041
Mn	0.054	0.002	0.001	0.001	0.005	0.026	0.000	0.032	0.000	0.000	0.002	0.016	0.000
Mg	0.532	0.347	0.496	0.000	0.084	1.311	0.454	1.113	0.348	0.001	0.419	1.471	0.628
Ca	0.499	0.449	0.007	0.001	0.004	0.579	0.488	0.604	0.378	0.000	0.003	0.802	0.636
Na	0.004	0.528	0.055	0.000	0.001	0.000	0.471	0.001	0.614	0.000	0.057	0.002	0.326
K	0.000	0.000	0.772	0.000	0.000	0.000	0.001	0.000	0.001	0.000	0.845	0.000	0.001
Total	8.023	4.033	6.868	1.004	1.993	7.996	3.982	8.023	4.056	2.995	6.938	8.012	3.982
$1X_{Fe^{3+}}$		0.460					0.000		0.687				0.000
$2X_{Fe^{3+}}$	0.035	0.359				0	0	0.052	0.704			0.048	0
K_{D1}	8.749					0		5.641				7.827	
K_{D2}	7.130					5.25		5.668				7.451	

(c)

	B589				B1015					B1058		
	Ky	Zo	Grt	Omp	Phn	Zo	Omp in/g	Grt in-r/Ky	Ky	Grt	Omp	Cpx sym
SiO_2	37.95	40.18	40.16	56.64	53.37	38.91	56.71	40.28	36.20	39.24	57.12	53.35
TiO_2	0.03	0.10	0.00	0.03	0.23	0.01	0.02	0.00	0.00	0.00	0.04	0.00
Cr_2O_3	0.03	0.00	0.00	0.00	0.00	0.00	0.01	0.00	0.00	0.00	0.03	0.02

Table 2. (*Continued*)

(c)

	B589				B1015					B1058		
	Ky	Zo	Grt	Omp	Phn	Zo	Omp in/g	Grt in-r/Ky	Ky	Grt	Omp	Cpx sym
Al_2O_3	62.87	31.02	22.70	9.48	23.16	32.00	11.35	22.54	62.01	22.05	12.53	4.27
FeO[a]	0.19	2.14	16.27	2.83	1.20	1.81	2.00	17.27	0.22	20.37	2.93	7.36
MnO	0.00	0.00	0.31	0.03	0.02	0.00	0.01	0.33	0.00	0.28	0.00	0.05
MgO	0.03	0.21	10.59	10.87	5.46	0.08	9.55	10.60	0.01	7.44	7.97	11.84
CaO	0.01	23.66	10.28	15.74	0.02	23.09	13.60	9.04	0.00	10.82	11.90	19.50
Na_2O	0.00	0.04	0.02	5.35	0.16	0.03	6.55	0.02	0.02	0.03	7.76	2.84
K_2O	0.00	0.02	0.00	0.00	10.66	0.00	0.01	0.01	0.00	0.00	0.01	0.01
Total	101.12	97.37	100.34	100.96	94.29	95.93	99.81	100.09	98.46	100.24	100.28	99.25
Si	1.012	6.134	2.990	1.991	3.576	6.021	1.997	3.009	0.993	2.991	2.003	1.979
Ti	0.001	0.012	0.000	0.001	0.011	0.001	0.001	0.000	0.000	0.000	0.001	0.000
Cr	0.001	0.000	0.000	0.000	0.000	0.000	0.000	0.000	0.000	0.000	0.001	0.001
Al	1.977	5.582	1.992	0.393	1.829	5.836	0.471	1.984	2.005	1.980	0.518	0.187
Fe^{3+}	0.004	0.273				0.234					0.009	
Fe^{2+}			1.013	0.083	0.067	0.000	0.059	1.079	0.005	1.298	0.077	0.228
Mn	0.000	0.000	0.020	0.001	0.001	0.000	0.000	0.021	0.000	0.018	0.000	0.002
Mg	0.001	0.048	1.176	0.569	0.546	0.018	0.502	1.180	0.001	0.845	0.417	0.654
Ca	0.000	3.870	0.820	0.593	0.002	3.828	0.513	0.723	0.000	0.884	0.447	0.775
Na	0.000	0.012	0.004	0.364	0.021	0.009	0.447	0.002	0.001	0.005	0.527	0.204
K	0.000	0.003	0.000	0.000	0.911	0.001	0.000	0.001	0.000	0.000	0.000	0.001
Total	2.996	15.934	8.015	3.994	6.964	15.948	3.991	8.000	3.005	8.022	4.001	4.030
$1X_{Fe^{3+}}$				0.000							0.109	
$2X_{Fe^{3+}}$			0.0457	0						0.150	0.013	
K_{D1}			5.887							8.311		
K_{D2}			5.6179							7.169		

X_{Fe3+}: $Fe^{3+}/(Fe^{3+} + Fe^{2+})$; 1, all Fe of Grt is assumed to be Fe^{2+} and Fe^{3+} = Na–Al for Cpx; 2, Fe^{3+} of Grt and Cpx was calculated by stoichiometry.

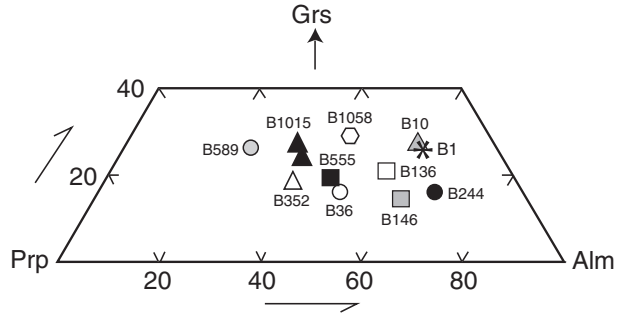

Fig. 4. Garnet compositions showing in Alm (+Sps)–Prp–Grs diagram.

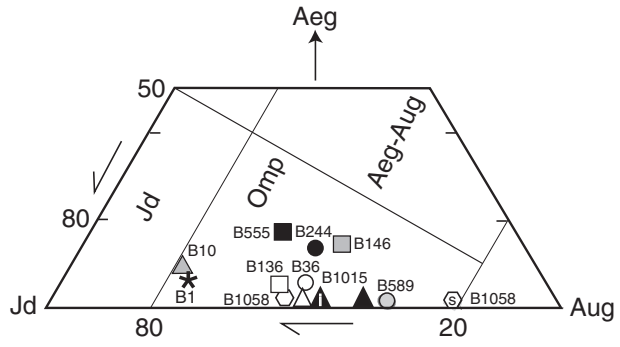

Fig. 5. Clinopyroxene compositions showing in Aug–Aeg–Jd diagram. i, inclusion; s, symplectite.

matrix mineral. Rutile inclusions are rounded or elongated 0.005–0.1 mm crystals, most clustering at the 0.01–0.04 mm size range. Matrix rutile grains of various shapes (see Fig. 3b–d) are either isolated intergranular prisms or aggregates consisting of several rutile crystals, and range from 0.05 to 0.6 mm in size (some up to >1 mm). Rutile is replaced by ilmenite, ilmenite + titanite or titanite along grain margins and fractures.

Compositions of rutile from 39 representative eclogite cores from 101 to 2774 m CCSD-MH depths were analysed (16–63 points for each sample). In addition to the major cation, the analysed rutile contain minor Zr, Nb, Al, Fe and Cr. Silicon and Mg, as major elements of eclogite, are negligible in rutile. Except for ~20% rutile lacking Al, rutile contains low Al concentrations (most data <200 ppm; however, several grains up to 520–1260 ppm), which are not listed in Table 3. Several trace elements in rutile are described below.

Zirconium contents of the matrix rutile show a large variation, ranging from 50 to 1020 ppm, with an average of 120–240 ppm; variations of Zr-in-rutile from retrograded eclogites are larger than those from fresh eclogites. Zr-in-rutile inclusions enclosed in garnet or omphacite range from 60 to 180 ppm, with an average of 100–160 ppm (Table 3). The variation of Zr contents in rutile with core depth is shown in Fig. 6. The rutile recording the highest Zr content is from an extensively retrograded eclogite; in this sample, Cpx has been totally replaced by a very fine-grained symplectite consisting of Pl + Amp (only garnet relics are preserved). This rutile, containing 1020 ppm Zr, is a relic enclosed in secondary ilmenite (Fig. 7).

Rutile is a major carrier of Nb. Niobium concentrations in rutile matrix grains range from 30 to

Table 3. Analyses of selected trace elements of rutile from CCSD Main Hole eclogites.

Units	Sample	Rock	Occurrence	n.o.a.	Zr (ppm)		Nb (ppm)		Cr (ppm)		Fe (wt%)	
					Range	Ave	Range	Ave	Range	Ave	Range	Ave
1	B1	Phn ecl	Matrix	38	90–540	150	460–1070	570	0–70	20	0.09–0.95	0.17
			Inc.	3	130–180	150	640–760	660	ND		0.12–0.34	0.20
	B10	Phn ecl	Matrix	18	90–170	120	210–340	280	ND		0.10–0.18	0.14
			Inc.	10	90–150	130	230–310	270	ND		0.12–0.20	0.15
	B25	t-ret ecl	Matrix	32	90–250	150	390–5960	2030	ND		0.26–1.41	0.36
			Inc.	4	90–160	120	1440–7190	3520	ND		0.34–0.43	0.37
	B36	Phn, Ky ecl	Matrix	16	80–170	120	250–340	290	160–560	400	0.08–0.18	0.13
			Inc.	7	80–170	120	280–330	300	130–280	190	0.11–0.32	0.19
	B49	s-ret ecl	Matrix	20	50–320	140	180–1510	510	ND		0.15–2.38	0.35
	B62	Phn ecl	Matrix	19	70–190	120	350–590	440	ND		0.10–0.84	0.20
			Inc.	8	60–130	100	390–440	420	ND		0.14–0.26	0.18
	B77	Phn ecl	Matrix	34	90–330	160	0–1450	640	ND		0.08–0.98	0.15
	B88	s-ret ky ecl	Matrix	24	100–1020	300	1100–4120	1610	ND		0.12–1.16	0.23
	B136	ecl	Matrix	27	70–200	140	0–160	120	0–70	40	0.21–0.80	0.30
			Inc.	3	80–130	110	130	130	0–100	40	0.30–0.36	0.32
	B146	ecl	Matrix	20	100–200	140	ND		ND		0.06–0.56	0.21
			Inc.	10	110–180	140	ND		ND		0.10–1.36	0.29
	B156	Phn ecl	Matrix	15	80–150	130	0–90	60	0–80	60	0.10–1.34	0.28
			Inc.	8	50–170	120	0–90	50	60–100	90	0.19–0.40	0.28
	B166	Phn ecl	Matrix	28	60–430	240	30–3060	790	ND		0.13–1.36	0.24
	B176	ecl	Matrix	6	130–190	150	680–730	710	ND		0.19–0.22	0.21
			Inc.	10	120–180	140	690–880	750	ND		0.32–0.47	0.37
	B196	s-ret ecl	Matrix	34	190–470	180	370–1870	560	ND		0.10–3.26	0.34
	B207	Phn ecl	Matrix	26	100–320	160	70–420	180	ND		0.09–0.42	0.14
			Inc.	4	90–110	100	150–180	160	ND		0.17–0.22	0.20
	B218	Phn ecl	Matrix	22	70–190	140	0–130	80	ND		0.05–0.87	0.15
			Inc.	2	120–130	125	70	70	ND		0.12–0.12	0.12
	B229	Phn ecl	Matrix	22	60–180	120	290–370	330	ND		0.12–0.19	0.13
	B244	ecl	Matrix	25	60–170	130	100–190	150	0–60	20	0.15–0.54	0.24
			Inc.	6	90–170	130	130–170	160	0–60	20	0.19–0.34	0.26
	B256	s-ret ecl	Matrix	16	100–460	160	850–12700	2750	ND		0.17–0.67	0.27
			Inc	10	70–150	100	1550–2000	1810	ND		0.26–0.38	0.32
2	B267	Pl-AM	Matrix	22	80–240	150	0–160	50	ND		0.18–4.17	0.44
			Inc	11	140–200	150	ND		0–70	50	0.13–0.26	0.18
4	B532	ecl	Matrix	22	60–190	140	0–70	20	50–110	80	0.15–2.52	0.31
	B555	Ky, Phn ecl	Matrix	25	90–240	130	260–600	390	110–210	160	0.15–1.72	0.31
	B589	s-ret Ky ecl	Matrix	22	90–220	130	330–2180	660	0–170	90	0.14–0.52	0.17
	B603	Pl-AM	Matrix	29	100–200	160	450–1510	740	ND		0.19–0.63	0.27
			Inc	2	140–180	160	470–490	480	ND		0.27–0.29	0.28
6	B829	Pl-AM	Matrix	28	80–160	130	250–490	340	100–170	140	0.12–1.68	0.24
	B854	ecl	Matrix	17	80–240	150	510–670	590	n/a		0.11–0.38	0.23
	B856	Phn ecl	Matrix	38	80–220	130	250–450	360	100–160	140	0.07–2.07	0.27
	B879	ret ecl	Matrix	30	90–380	160	250–550	390	90–160	130	0.13–1.77	0.29
			Inc	3	110–130	120	310–330	320	120–140	130	0.34–0.36	0.35
	B899	Phn ecl	Matrix	33	90–210	130	170–440	310	110–180	160	0.05–1.90	0.15
			Inc	2	140–140	140	240–250	250	160–180	170	0.15–.16	0.16
	B909	Phn ecl	Matrix	18	50–190	130	150–310	240	170–200	190	0.13–0.95	0.21
			Inc	9	110–160	140	220–260	240	180–230	200	0.10–0.30	0.22
	B919	Phn ecl	Matrix	24	90–190	140	130–280	200	70–180	150	0.08–2.33	0.21
			Inc	4	70–150	105	210–250	230	130–160	150	0.15–0.45	0.24
	B992	Phn ecl	Matrix	33	60–190	140	220–550	290	100–170	130	0.05–2.47	0.26
	B1015	Ky, Phn ecl	Matrix	36	80–190	140	160–260	230	80–160	140	0.11–0.34	0.16
	B1040	ecl	Matrix	23	60–310	120	270–400	320	n/a		0.26–0.70	0.40
	B1058	ecl	Matrix	42	60–340	160	170–1260	360	ND		0.18–0.39	0.24
			Inc	3	130–160	140	210–280	250	ND		0.25–0.31	0.27
7	B1399	ecl	Matrix	62	80–320	170	310–870	450	120–510	160	0.12–3.05	0.21
			Inc	1	140		540		150		0.24	

Ecl, eclogite; Pl-AM, plageoclase amphibolite (retrograded from eclogite); ret, retrograde; s-ret, strongly retrograde; t-ret, totally retrograded; inc, inclusion; n.o.a., numbers of analysis; ave, average; ND, not detected; n/a, not analysed.

12 700 ppm except for a few Nb-free analyses; the average Nb contents range from 200 to 2750 ppm and most analyses cluster ~200–750 ppm (Nb-free analyses were not included in this average). Rutile inclusions contain 210–7190 ppm Nb, with an average range of 250–3520 ppm. The host rocks of Nb-free rutile are Fe–Ti-rich eclogites with very low Nb (most < 3 ppm) from units 2 and 1 (Zhang *et al.*, 2006b). In addition, the rutile grains with high-Nb content (> 1000 ppm) were found in strongly retrograded eclogites, in which most omphacite is replaced by Pl + Amp, and garnet is partially replaced by Amp + Pl ± Ep ± Bt, such as sample B25, B88, B196, B256, B589. Definitely, the variations of Nb concentrations in rutile reflect bulk-rock compositions and the latter modification by metasomatic processes during decompression overprinting.

In addition to Zr and Nb, rutile also contains minor Fe, Cr and Al. The iron is a major trace element in rutile, ranging from 0.05 to 4.17 wt% (average of 0.12–0.44 wt%). The high-Fe contents (> 1wt%) are

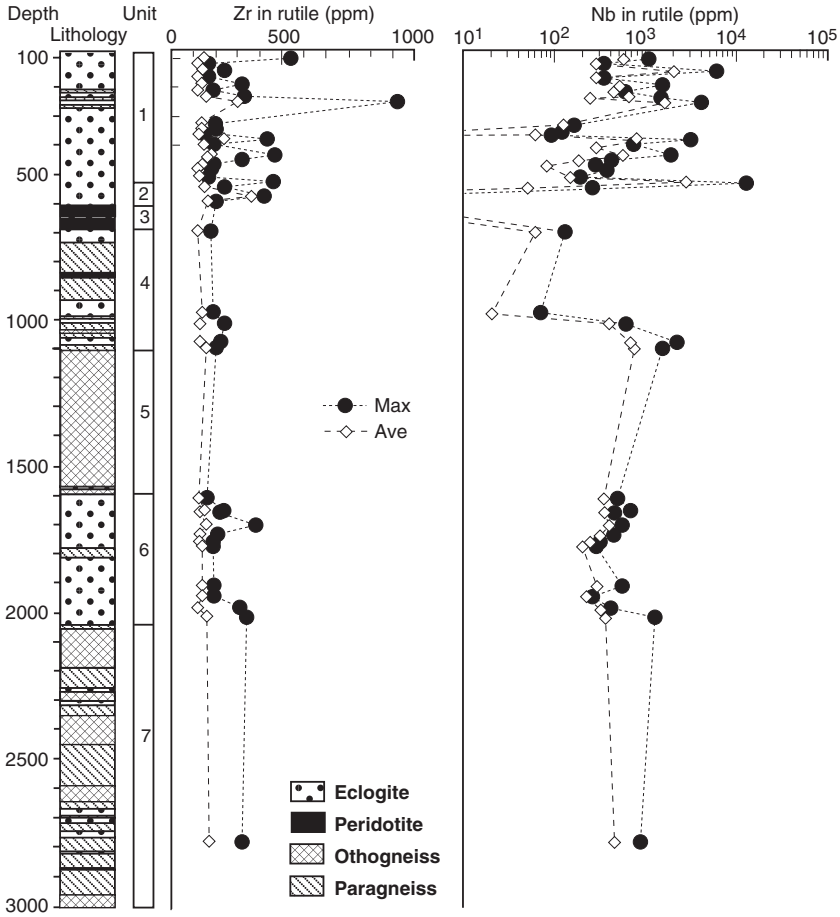

Fig. 6. Average and maximum Zr and Nb concentrations of rutile from CCSD-MH eclogites.

exceptions, and probably result from mixtures with undetected inclusions of very tiny ilmenite or iron oxide lamellae or exsolved films. The Cr contents in rutile range from 0 to 510 ppm. It is worth noting that rutile from units 1 and 2 is mostly Cr-free; in contrast, except for a few samples, the rutile from units 4 to 7 contains Cr values of 70–450 ppm. The relation between bulk composition and Cr content in rutile is indistinct because of lack of bulk-rock compositional data for these samples and the major carriers of Cr are garnet and omphacite, not rutile in eclogite.

P–T ESTIMATES

The Fe^{2+}–Mg exchange thermometer for coexisting garnet and clinopyroxene requires an accurate estimate of the Fe^{2+} and Fe^{3+} contents of garnet and omphacite, particularly for Fe-poor omphacite, because even fairly small variations in any of the analysed elements may give substantial variations in the Fe^{2+}/Fe^{3+} ratio based on stoichiometry (Krogh Ravna, 2000). In this study, two methods were used to calculate the Fe^{3+} of eclogitic omphacite and garnet: (i) for clinopyroxene, if Na > Al, Fe^{3+} = Na–Al (Cr can be ignored in the MH eclogites), and if Na ≤ Al, all Fe = Fe^{2+} based on six oxygen ions; for garnet, all Fe is assumed to be Fe^{2+} based on 12 oxygen ions inasmuch as their Fe^{3+} contents are negligible and (ii) Fe_2O_3 contents of garnet and omphacite were calculated based on eight and four cations respectively. The compositional data listed in Table 2 are results from using the first method, but $Fe^{3+}/(Fe^{2+} + Fe^{3+})$ ratios and Fe–Mg partitioning coefficients between garnet and clinopyroxene by using the two methods are also shown in Table 2. The Zr-in-rutile thermometer was applied to all eclogites.

Application of the Zr-in-rutile thermometer

Rutile occurs in virtually all eclogites. Therefore, the Zr-in-rutile thermometer represents a powerful tool to estimate the temperatures of eclogite metamorphism, especially in cases where omphacite has been totally replaced by secondary plagioclase and amphibole. The studied eclogites are coesite-bearing (or exhibit quartz pseudomorphs after coesite) rocks that, by definition, experienced UHP metamorphism. Typically, eclogitic zircon consists of a magmatic core and a metamorphic mantle and/or rim. The metamorphic domain contains inclusions of garnet, omphacite, phengite, coesite and rutile (Zhang *et al.*, 2006b,c; Liu *et al.*, 2008). The zircon apparently was in equilibrium with eclogitic rutile, even though zircon and rutile are not in direct

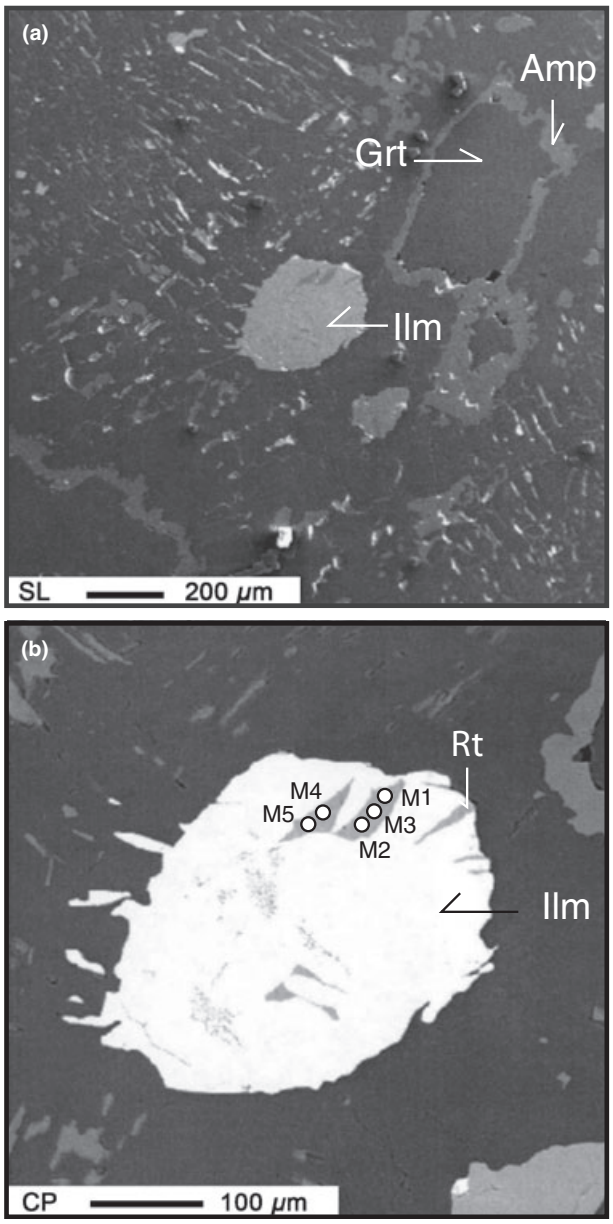

Fig. 7. Relict rutile with high-Zr concentration in ilmenite (a), and its large view with analyzed points is shown in (b). SL, secondary electron reflect image CP, back-scattered electron image. M1–M5, analysis points: Zr contents (ppm) are 390, 1020, 760, 860 and 780 from M1 to M5 respectively.

contact as a result of the scarcity of zircon in comparison with rutile. Calculated temperatures for coesite/quartz-bearing CCSD-MH eclogites employing three Zr-in-rutile thermometers (Zack *et al*., 2004; Watson *et al*., 2006; Tomkins *et al*., 2007) are listed in Table 4, and the variation of temperature with depth is depicted in Fig. 8. Except for B88 (a totally retrograded eclogite), the maximum and average temperatures are 645–794 and 595–678 °C obtained by the calibration of Zack *et al*. (2004) and 595–693 and 570–618 °C by that of Watson *et al*. (2006) respectively. The average temperature estimates result in relative low-T values that reflect conditions of the various stages. For fresh eclogites, the differences between average and maximum temperatures are smaller than those of strongly overprinted eclogites (Fig. 8); evidently retrograde metamorphism may have modified the rutile compositions.

The two Zr-in-rutile thermometers described above do not consider pressure influence on Zr substitution in rutile. At high pressure, the larger Zr^{4+} (ionic radius = 0.72 Å) cation will be less able to substitute for the smaller Ti (0.61 Å). Another thermometer (Tomkins *et al*., 2007) that accounts for the effect of pressure (temperature will rise ~20 °C with a pressure increase of 10 kbar) was employed to calculate temperatures of rutile formation at 40 kbar for the UHP eclogites (Table 4). The estimated maximum temperatures at 40 kbar are 705–811 °C for unit 1, 734 °C for unit 2 (only one sample), 714–734 °C for unit 4, 700–766 °C for unit 6, 781 °C for unit 7; but only one sample is available for units 2 and 7. These estimates at 40 kbar give 17–61 °C higher than the maximum temperature calculated by the Zack thermometer (Zack *et al*., 2004) (Table 4). The highest Zr content in rutile (sample B88, an extensively retrograded eclogite) yields a temperature of 879 °C at 40 kbar, however, the highest Zr contents were obtained from relict rutile that is almost totally replaced by ilmenite (see Fig. 7); if the five analyses (390–1020 ppm) of rutile relicts are excluded, Zr contents (19 analyses) of eight matrix rutile grains range from 100 to 370 ppm and the maximum temperature would be 774 °C, which is only 28 °C higher than the maximum temperature calculated by the Zack *et al*., (2004) thermometer.

Fe^{2+}–Mg exchange thermometer

In order to compare the Zr-in-rutile and Fe–Mg exchange thermometers the equilibrium temperature of coexisting garnet and omphacite were also calculated for representative eclogites using the Grt–Cpx thermometer**.** Eclogites selected for chemical analyses of minerals are mostly less retrograded except for kyanite-bearing eclogite samples B555 and B589. As described above, most garnet and omphacite in individual sample have homogenous compositions, or compositional variation between cores and rims are very limited (±1–2%, this study and Zhu *et al*., 2007). At the boundaries between garnet and omphacite in direct contact lack pronounced composition gradients. These characteristics indicate the compositions in the studied samples have not been significantly reset due to kinetic factor during exhumation. The estimated P–T conditions by core–mantle compositions approximately represent peak or close to peak P–T conditions. In this study, the geothermobarometry for Grt–Cpx–Ky–Phn–Coe/Qtz parageneses (Krogh Ravna & Terry, 2004) was applied to estimate P–T conditions of phengite-, kyanite- and phengite–kyanite-bearing

Table 4. Estimated temperatures of CCSD main hole eclogites.

Unit	Sample no.	Rock type	Depth (m)	n.o.a.	Zr-in-rutile termometry (°C)					
					WWT		ZMK		TPE (40 kbar)	
					Ave	Max	Ave	Max	Ave	Max
1	B1	ecl	101	41	585	693	622	794	690	811
	B10	ecl	118	28	574	598	603	646	679	705
	B25	ecl	142	36	592	628	635	696	693	738
	B36	ecl	164	23	572	598	599	646	677	705
	B49	ecl	189	20	582	648	615	727	689	760
	B62	ecl	211	27	570	607	595	661	673	714
	B77	ecl	232	34	591	673	632	765	700	788
	B88[a]	ecl	249	19	600	660	649	746	707	774
	B136	ecl	326	30	580	611	613	667	687	719
	B146	ecl	342	30	587	611	626	667	689	719
	B156	ecl	359	23	573	598	600	646	681	705
	B166	ecl	376	29	618	673	678	765	734	788
	B176	ecl	393	16	585	607	622	661	691	714
	B196	ecl	429	34	595	681	639	776	710	797
	B207	ecl	446	30	586	648	623	727	695	760
	B218	ecl	463	24	580	607	613	661	689	714
	B229	ecl	479	22	571	603	596	654	677	710
	B244	ecl	502	31	578	598	609	646	683	705
	B256	ecl	522	26	578	679	609	774	686	795
2	B267	Pl-AM[b]	541	22	588	625	627	690	695	734
4	B532	ecl	968	22	581	607	615	661	689	714
	B555	ecl	1005	25	577	625	608	690	683	734
	B589	ecl	1068	22	580	618	613	679	683	727
	B603	Pl-AM[b]	1089	31	592	614	636	673	700	719
6	B829	Pl-AM[b]	1601	28	578	594	610	639	683	700
	B854	ecl	1644	17	584	623	620	688	695	734
	B856	ecl	1649	32	579	618	611	679	683	727
	B879	ecl	1692	33	587	662	625	749	698	776
	B899	ecl	1726	35	580	614	613	673	684	723
	B909	ecl	1751	28	578	607	608	661	685	714
	B919	ecl	1767	28	580	607	613	661	686	714
	B992	ecl	1900	30	580	614	616	673	689	714
	B1015	ecl	1935	36	582	607	618	661	689	714
	B1040	ecl	1976	24	570	645	593	724	677	757
	B1058	ecl	2007	45	591	653	632	735	699	766
7	B1399	ecl	2774	63	596	666	643	756	705	781

[Zr-in-rutile thermometry] WWT: Watson *et al*., 2006; ZMK: Zack *et al*., 2004; TPE: Tomkins *et al*., 2007.
[a]Five analyses of rutile relics in sample B88 shown in Fig. 7 were not included for *T* calculation.
[b]Pl-amphibolite (retrograded from eclogite)

eclogites. For eclogites with or without kyanite and phengite, temperatures were calculated at a given average pressure of ~40 kbar employing the Fe^{2+}–Mg exchange thermometer of Grt–Cpx (Ai, 1994; Krogh Ravna, 2000). All *P–T* estimates for the selected eclogites are listed in Table 5.

Phengite-, kyanite- and phengite–kyanite-bearing eclogites yield *P–T* estimates of 655–919 °C and 34–50 kbar (Table 5), consistent with the *P–T* estimates from other MH core samples (Zhang *et al*., 2006b). Calculated temperatures of 684–853 °C (assuming Fe^{3+} in omphacite = Na–Al) at 40 kbar using the Ai (1994) thermometer are nearly identical to the temperature estimate (693–845 °C) by the Krogh Ravna calibration (Krogh Ravna, 2000). Where Fe_2O_3 contents in both garnet and omphacite are calculated by the second method described above, the calculated $Fe^{3+}/(Fe^{2+} + Fe^{3+})$ values of garnet range from 0.0 to 0.07, and that of omphacite range from 0 to 0.50 with two exceptions, which, in most cases, are higher than the ratios assuming Fe^{3+} = Na–Al (Table 2). In most cases, the $Fe^{3+}/(Fe^{2+} + Fe^{3+})$ ratios calculated by stoichiometry give relatively low Fe–Mg petitioning coefficients (K_{D2}) (see Table 2 and Fig. 9), and in turn, yield relatively high temperatures. Fortunately, for most samples, the variations in temperature are not significant.

DISCUSSION

Zirconium in rutile inclusions

In the studied eclogitic rutile, variations of Zr contents in most fresh samples are limited. Zirconium concentrations in rutile inclusions in garnet and omphacite are not higher than those of intergranular rutile grains in the matrix, unlike results reported by Zack *et al*. (2004). The average (100–160 ppm) and maximum Zr contents (200 ppm) of the inclusions are lower than those (average 120–240 ppm and maximum 554 ppm) of the matrix rutile except for the highest Zr values in rutile relics from heavily retrograded eclogites. These data indicate that the inclusions did not record the maximum peak temperatures, but must have formed before or close to the peak stage of UHP metamorphism, probably as diffusional reequilibration was not

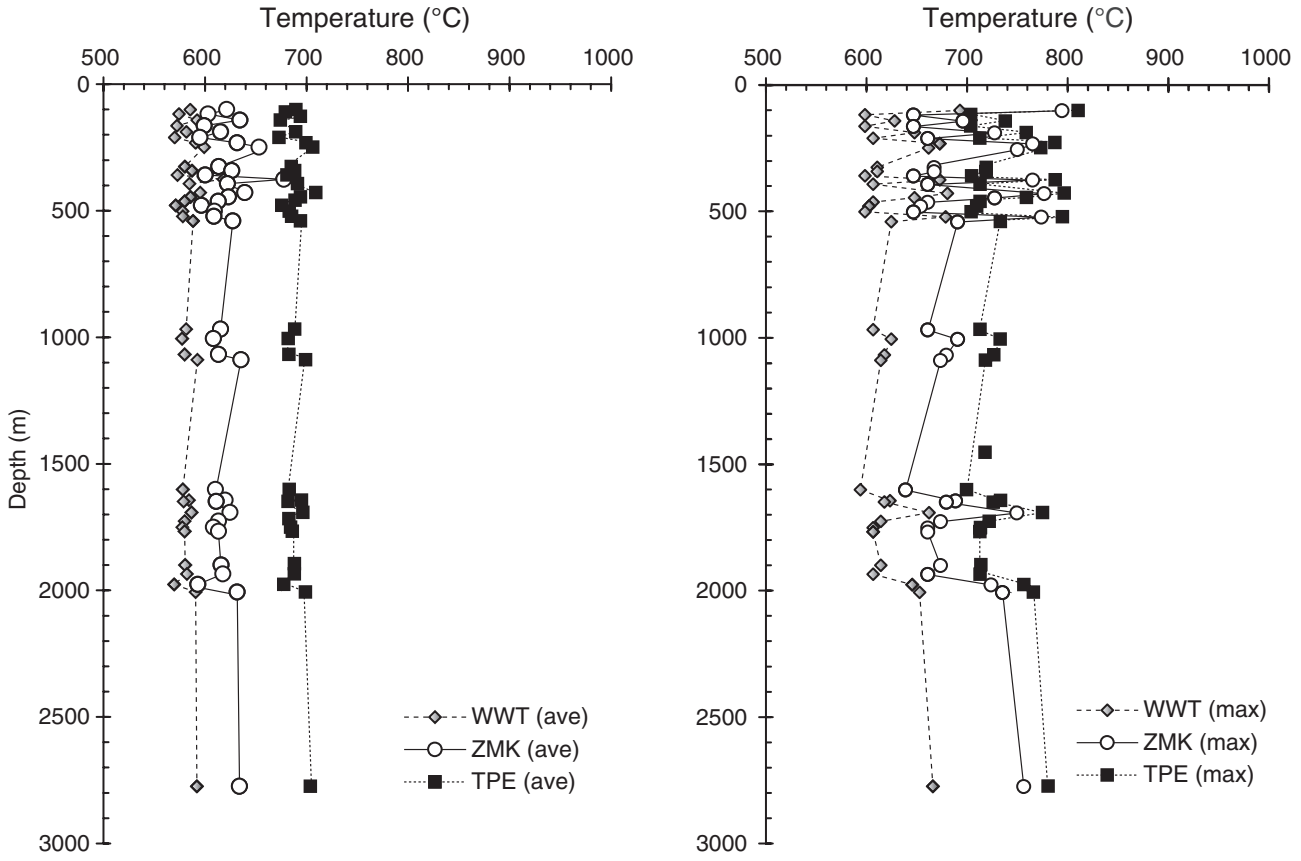

Fig. 8. Comparison of maximum and average temperature estimates of three Zr-in-rutile thermometers (Zack *et al.*, 2004; Watson *et al.*, 2006; Tomkins *et al.*, 2007) for CCSD-MH eclogites.

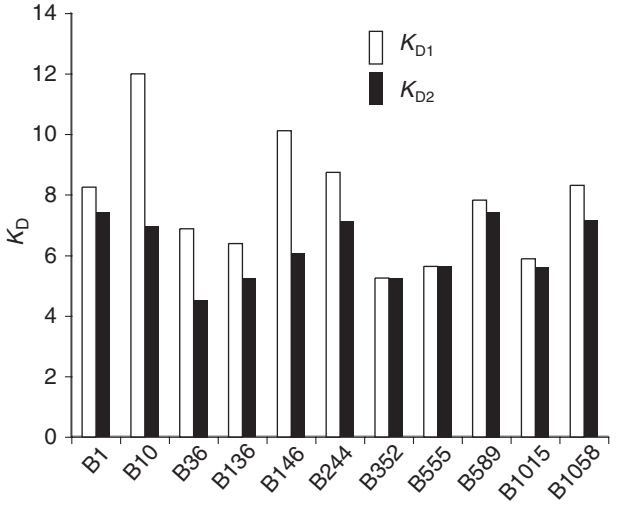

Fig. 9. Comparative Fe–Mg partitioning coefficient (K_D) between garnet and clinopyroxene using different Fe^{3+} calculation. The stoichiometry calculation for garnet and clinopyroxene yield lower values (K_{D2}) than those (K_{D1}) of Fe^{total} of garnet express as FeO and Fe^{3+} = Na–Al for clinopyroxene.

completed at peak temperature. The rate of Zr diffusion in rutile is slow in comparison with Cr, Sc, Mn and Fe (Cherniak, 2000) and Zr diffusion in the garnet crystal lattice is also very slow (Zack *et al.*, 2002). Curiously, the highest Zr content with the largest variation (100–1020 ppm) for the matrix rutile occurs in a strongly retrograded eclogite (B88), in which the Nb content in the rutile is also high (1100–4120 ppm). To minimize retrogression effects, these anomalous high-Zr and high-Nb analyses were excluded from calibration of the rutile thermometer for the CCSD-MH eclogites. The unusually high contents of Zr and Nb in rutile (especially Nb) in the strongly retrograded eclogite may reflect the infiltration of fluids; moreover, the retrograde rutile probably did not achieve equilibrium with the coexisting zircon.

Fe–Mg exchange *v.* Zr-in-rutile thermometer

The compositions of both garnet and Cpx calculated by stoichiometry (Fe^{3+} approximated by the second method) normally yielded a higher temperature estimate of 0–175 °C with an average ~55 °C greater than that assuming Fe^{3+} = Na–Al in Cpx and Fe^{3+} absent in garnet at 40 kbar (Table 5). The *P–T* estimates by Grt–Cpx–Ky–Phn geothermobarometry (Krogh Ravna & Terry, 2004) are 34–50 kbar with a large variation in temperature; the variation, to a certain extent, depends on the uncertainty of Fe^{3+} calculation.

Table 5. *P–T* estimates of CCSD-MH eclogites.

Sample no.	Grt–Cpx				Grt + Cpx + Phn ± Ky		Zr-in-rutile	
	Ai (1994)		Krogh Ravna (2000)		Krogh Ravna & Terry (2004)		Tomkins *et al.* (2007) at 40 kbar	
	Fe^{3+} = stoic	Fe^{3+} = Na–Al	Fe^{3+} = stoic	Fe^{3+} = Na–Al				
	40 kbar		40 kbar		*T* (°C)	*P* (kbar)	Average	Maximum
Unit1								
B1(ZM)[a]	837	741	832	793	843	44	695	811
B10	867	691	862	693	919	50	677	705
B36	880	712	890	737	901	42	677	705
B136	899	818	897	819			689	716
B146	772	615	784	632			689	719
B244	751	684	756	691	719	34	683	705
Unit 2								
B352	816	816	818	818				
B555	813	813	818	818	665	35	683	734
B589	732	716	735	719	728	41	683	727
Unit 6								
B1015	874	853	863	845	684	40	689	714
B1058	832	778	824	773			689	700

Stoic, stoichiometry (formulae of Grt and Cpx were calculated based on 8 and 4 cations, respectively).
[a]Mineral compositions from Zhang *et al.* (2006b).

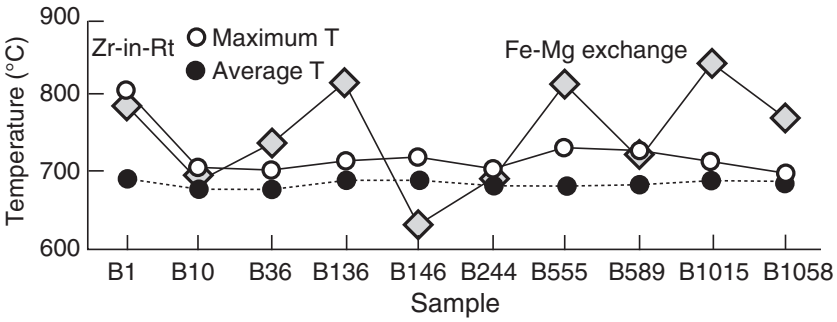

Fig. 10. Temperature calculations by Zr-in-rutile (Zack *et al.*, 2004) and Fe–Mg partitioning (Krogh Ravna, 2000, Fe^{3+} = Na–Al) thermometers for the same samples.

In the calibration of Krogh Ravna & Terry (2004), Fe^{3+}/Fe^{total} ratios of garnet, phengite and Cpx are based on charge balance; this method is very sensitive to the quality of the chemical analyses of minerals (Carswell & Zhang, 1999). In addition, under HP/UHP conditions, clinopyroxene may be non-stoichiometric because of the presence of Ca-Eskola $Ca_{0.5}AlSiO_6$ component (Krogh Ravna & Paquin, 2003) or defects in mineral structure. In general, assuming Fe^{3+} = Na–Al, the calculated temperatures are close to the maximum temperatures estimated by the Zr-in-rutile thermometer.

For Zr-in-rutile thermometers, calibrations by Watson *et al.* (2006) and Tomkins *et al.* (2007) yielded the lowest and the highest temperatures respectively. The maximum temperature (639–794 °C) obtained by empirical calibration of the rutile thermometer (Zack *et al.*, 2004) and the maximum temperature (700–811 °C) estimated at 40 kbar using the Tomkins *et al.* (2007) thermometer for all rutile in the analysed CCSD-MH eclogites are comparable; differences are limited to 17–59 °C and in most cases, the Tomkins *et al.* (2007) thermometer gives a slightly higher temperature than that by Zack *et al.* (2004). The comparison between Fe–Mg exchange and Zr-in-rutile thermometers is shown in Fig. 10. Except for two samples (B136 & B1015), at a pressure of 40 kbar and Fe^{3+} = Na–Al, the differences of temperature estimates by the Fe–Mg exchange thermometer (Krogh Ravna, 2000) and the maximum temperature estimates by the Zr-in rutile thermometer (Tomkins *et al.*, 2007) are $< \pm 85$ °C. The Zr-in-rutile thermometer might be commonly applied to systems with coexisting quartz and zircon, and the maximum temperature may represent the peak temperature for fresh eclogite. If the Zr concentrations in rutile were analysed over a large area, a quantitative picture of the thermal structure of the UHP terrane would be expected.

Thermal structure of the Triassic subduction zone

In addition to Fe–Mg exchange thermometer and Grt–Cpx–Ky–Phn geothermobarometry, the Zr-in-rutile thermometers were applied to estimate systematically the temperature of formation of eclogites from 100 to 3000 m depth in the CCSD-MH. The MH samples provide a remarkable opportunity to examine the fossil thermal structure of the documented 3-km thick Sulu

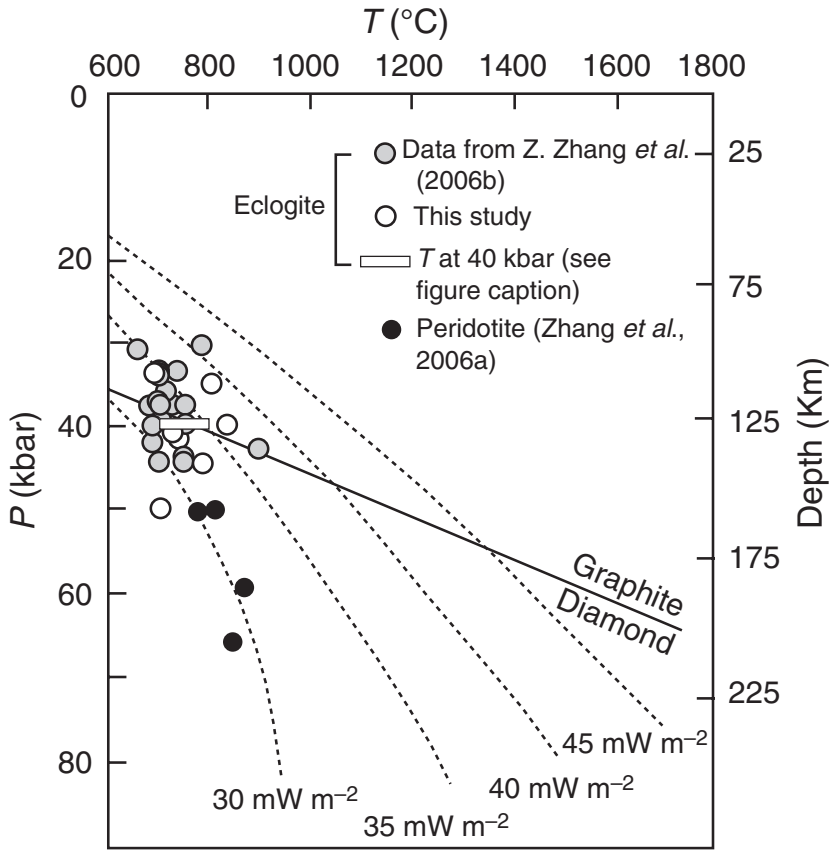

Fig. 11. Sulu UHP rock-based empirical geotherm. Conductive model geotherm (dashed lines) for different surface heat flow values, after Pollack & Chapman (1977). In this diagram, pressure is estimated by Grt–Omp–Phn–Ky geobarometer (Krogh Ravna & Terry, 2004) and temperature is calculated by Grt–Cpx thermometer (Krogh Ravna, 2000) assuming Fe^{3+} = Na–Al in omphacite. The open bar represents the estimated temperatures at 40 kbar suing the Zr-in-rutile thermometer (Tomkins *et al.*, 2007) for the main hole eclogites.

UHP slab. Computed metamorphic temperatures exhibit no distinct variation in the slab: the maximum average temperature at 40 kbar is 743 °C for unit 1 (100–530 m), 734 °C for unit 2 (530–600 m), 724 °C for unit 4 (680–1160 m), 731 °C for unit 6 (1600–2190 m), and 781 °C for unit 7 at 2774 m. Relatively higher temperature estimates averaging 743 °C were obtained from unit 1. The eclogite in unit 7 at 2774 m also shows a high-*T* estimate of 781 °C; unfortunately only one sample is available. Slightly lower temperature calculations were obtained for eclogites in a shear zone between 870 and 1113 m within unit 4 (Xu *et al.*, 2004), which probably was caused by strong deformation that enhanced fluid infiltration and retrogression. Abundant coesite inclusions in garnet and zircon from eclogite and gneiss between depths of 100 and 5150 m, and from the surface in an area of > 5000 km^2 of the southern Sulu terrane (Liu *et al.*, 2007) suggest the existence of an at least 3-km thick slab that crystallized at more-or-less constant temperature.

Judging from *P–T* estimates (830–900 °C, 15–17 kbar) of spinel lherzolite, spinel harzburgite and websterite xenoliths within late Cenozoic basanites in the Donghai area, Jin *et al.* (2003) constructed a xenolith-based geotherm, corresponding to a continental heat flow value of 75 mW m^{-2}. CCSD-MH peridotites are interlayered with eclogites between the depths of 603–683 m, and metamorphosed at 50–70 kbar, 780–900 °C (Zhang *et al.*, 2006a). If all the data are combined including the *P–T* estimates of the CCSD-MH eclogites in this study and the previously published *P–T* data by Zhang *et al.* (2006b) and Zhu *et al.* (2007) with the *P–T* estimates of CCSD-MH peridotites, this would allow a regional geotherm of the Triassic subduction zone between the Sino-Korean and Yangtze cratons to be constructed. Results of *P–T* estimate yield a low thermal gradient of $\sim$5 °C km^{-1}, which is in accord with the 30–35 mW m^{-2} model conductive geotherms (Fig. 11) (Pollack & Chapman, 1977), and distinctly lower than the Cenozoic xenolith-derived geotherm (Jin *et al.*, 2003).

CONCLUSIONS

The CCSD-MH eclogites interlayered with gneisses from depths of 100–3000 m include phengite-, kyanite-, zoisite/epidote-bearing and bi-mineralogical eclogites. Quartz (or coesite) is present in most eclogites; quartz-free eclogite is rare and only occurs enclosed in peridotite layers. Analyses of selected elements (Ti, Mg, Si, Al, Zr, Nb, Cr & Fe) for rutile from 39 eclogite cores indicate that rutile is Si and Mg free, and the most common substitutional impurities in rutile are Nb, Zr and Fe. A few rutile contain trace concentrations of Al and Cr. The Nb concentration in rutile is mainly controlled by bulk-rock composition, but may have

been modified by fluid infiltration during retrograde overprinting.

Zirconium concentration in the matrix rutile ranges from 50 to 540 ppm, except for sample B88, averaging 120–240 ppm. Compared with rutile in the matrix, rutile inclusions have somewhat lower Zr contents (50–200 ppm; average: 100–160 ppm), indicating that the rutile inclusions grew prior to reaching or close to the maximum temperature of UHP metamorphism.

For the Sulu UHP eclogites, three Zr-in-rutile thermometers yielded temperature estimates characterized by differences of several tens of °C. The computed values do not show a distinct variation or temperature gap, suggesting that these rocks from 100 to 3000 m (even 5000 m) depth lie within a single thick UHP slab. In most cases, the maximum temperatures of 700–811 °C calculated at 40 kbar (average pressure) by the Zr-in-rutile thermometer (Tomkins *et al*., 2007) are comparable to the temperature estimated by Fe–Mg partitioning between garnet and clinopyroxene (assuming Fe^{3+} = Na–Al) at 40 kbar (Ai, 1994; Krogh Ravna, 2000). Therefore, only the maximum temperature estimated at the actual peak pressure represents the true peak temperature. These data combined with published *P–T* calculations for CCSD-MH eclogites and peridotites yield a low thermal gradient ($\sim$5 °C km^{-1}) giving a $\sim$30–35 mW m^{-2} model conductive geotherm (Pollack & Chapman, 1977) for the subduction zone juxtaposing the Sino-Korean and Yangtze cratons (Fig. 11). This geotherm is distinctly lower than the Cenozoic xenolith-derived geotherm (Jin *et al*., 2003).

ACKNOWLEDGEMENTS

We sincerely thank the Laboratory of Continental dynamics, Institute of Geology, Chinese Academy of Geological Sciences for providing a great number of thin sections of eclogite and gneiss from CCSD-MH cores. We much appreciate E.J. Krogh Ravna for his excel version for our *P–T* calculation and for the helpful review of this manuscript by two anonymous reviewers. This research was supported by NSF EAR-0003355, EAR-0506901 and EAR-0810969, and partially by National Taiwan University and JSPS Grant-in-Aid for Scientific Research (B) (21340148).

REFERENCES

Ai, Y., 1994. A revision of the garnet-clinopyroxene Fe^{2+}–Mg exchange geothermometer. *Contributions to Mineralogy and Petrology*, **115,** 467–473.

Carswell, D. A. & Zhang, R. Y., 1999. Petrographic characteristics and metamorphic evolution of ultra-high pressure eclogites in plate collision belts. *International Geology Review*, **41,** 781–798.

Chen, R. X., Zheng, Y. F., Zhao, Z. F., Tang, J., Wu, F. Y. & Liu, M., 2007. Zircon U–Pb age and Hf isotope evidence for contrasting origin of bimodal protoliths for ultrahigh-pressure metamorphic rocks from the Chinese Continental Scientific Drilling project. *Journal of Metamorphic Geology*, **25,** 873–894.

Cherniak, D. J., 2000. Pb diffusion in rutile. *Contributions to Mineralogy and Petrology*, **139,** 198–207.

Ferry, J. M. & Watson, E. B., 2007. New thermodynamic models and revised calibrations for the Ti-in-zircon and Zr-in-rutile thermometers. *Contributions to Mineralogy and Petrology*, **154,** 429–437.

Hacker, B. R., Ratschbacher, L. & Liou, J. G., 2004. Subduction, collision, and exhumation in the ultrahigh-pressure Qinling-Dabie Orogen: a review. In: *Aspects of the Tectonic Evolution of China, Special Publication 226*, (ed. Malpas, J.), pp. 157–175, Geological Society, London.

Jahn, B.-M., Fan, Q., Yang, J. J. & Henin, O., 2003. Petrogenesis of the Maowu pyroxenite–eclogite body from the UHP metamorphic terrane of Dabieshan: chemical and isotopic constraints. *Lithos*, **70,** 23–267.

Jin, Z., Yu, R., Yang, W. & Ou, X., 2003. Mantle-derived xenoliths of peridotite from Pingmingshan, Donghai County, Jiangsui Province, and their implications for deep structure. *Acta Geologica Sinica*, **7,** 451–462 (in Chinese with English abstract).

Kretz, R., 1983. Symbols for rock-forming minerals. *American Mineralogist*, **68,** 277–279.

Krogh Ravna, E., 2000. The garnet–clinopyroxene Fe^{2+}–Mg geothermometer: an update calibration. *Journal of metamorphic Geology*, **18,** 211–219.

Krogh Ravna, E. J. & Paquin, J., 2003. Thermobarometric methodologies applicable to eclogites and garnet ultrabasites. *European Mineralogical Union Notes in Mineralogy*, **5,** 229–259.

Krogh Ravna, E. J. & Terry, M. P., 2004. Geothermobarometry of UHP and HP eclogites and schists – an evaluation of equilibria among garnet–clinopyroxene–kyanite–phengite–coesite/quartz. *Journal of Metamorphic Geology*, **22,** 579–592.

Liu, F. & Xu, Z., 2005. U–Pb SHRIMP ages recorded in the coesite-bearing zircon domains of paragneisses in the southwestern Sulu terrane, eastern China. New Interpretation. *American Mineralogist*, **90,** 790–800.

Liu, F., Xu, Z. & Liou, J. G., 2004. SHRIMP U–Pb ages of ultrahigh-pressure and retrograde metamorphism of gneisses southwestern Sulu terrane, eastern China. *Journal of Metamorphic Geology*, **22,** 315–326.

Liu, F., Gerdes, A., Liou, J. G., Xue, H. & Liang, F. H., 2006. SHRIMP U–Pb zircon dating from Sulu-Dabie dolomitic marble, eastern China: constraints on the prograde, UHP and retrograde metamorphic ages. *Journal of Metamorphic Geology*, **24,** 569–589.

Liu, F., Xu, Z., Liou, J. G., Dong, H. & Xue, H., 2007. Ultrahigh-pressure mineral assemblages in zircons from surface to 5158 m depth cores in the main drill hole of Chinese Continental Scientific Drilling Project, southwestern Sulu belt, China. *International Geological Review*, **49,** 454–478.

Liu, F., Gerdes, A., Zeng, L. & Xue, H., 2008. SHRIMP U–Pb dating, trace elements and the Lu–Hf isotope system of coesite-bearing zircon from amphibolite in the SW Sulu UHP terrane, eastern China. *Geochimica et Cosmochimica Acta*, **72,** 2973–3000.

Pollack, H. N. & Chapman, D. S., 1977. On the regional variation of heat flow, geotherms and lithospheric thickness. *Tectonophysics*, **38,** 279–296.

Reed, S. J. B., 1993. *Electron Microprobe Analysis*, 2nd edn. Cambridge University Press, Cambridge, 326 pp.

Tomkins, H. S., Powell, R. & Ellis, D. J., 2007. The pressure dependence of the zirconium-in-rutile thermometer. *Journal of Metamorphic Geology*, **25,** 703–713.

Watson, E. B., Wark, D. A. & Thomas, J. B., 2006. Crystallization thermometers for zircon and rutile. *Contributions to Mineralogy and Petrology*, **151,** 413–433.

Xu, Z., Zhang, Z., Liu, F. *et al*., 2004. The structure profile of 0-1200 m in the main borehole, Chinese Continental Scientific

Drilling and its preliminary deformation analysis. *Acta Petrologic Sinica*, **20,** 53–72 (in Chinese with English abstract).
Yang, J. J. & Jahn, B. M., 2000. Ultra-deep subduction of the Su-Lu garnet peridotite and its isotopic and mineral chemical consequences. *Journal of Metamorphic Geology*, **18,** 167–180.
Yang, J. S., Xu, Z. Q., Dobrzhinetskaya, L. F. *et al*., 2003. Discovery of metamorphic diamonds in central Chin: an indication of a >4000-km-long zone of deep subduction resulting from multiple continental collisions. *Terra Nova*, **15,** 370–379.
Zack, T., Kronz, A., Foley, S. F. & Rivers, T., 2002. Trace element abundances in rutiles from eclogites and associated garnet mica schists. *Chemical Geology*, **184,** 97–122.
Zack, T., Morace, R. & Kronz, A., 2004. Temperature dependence of Zr in rutile: empirical calibration of a rutile thermometer. *Contributions to Mineralogy and Petrology*, **148,** 471–488.
Zhang, R. Y., Hirajima, T., Banno, S., Cong, B. & Liou, J. G., 1995. Petrology of ultrahigh-pressure rocks from the southern Sulu region, eastern China. *Journal of Metamorphic Geology*, **13,** 659–675.
Zhang, R. Y., Liou, J. G., Yang, J. S. & Yui, T. F., 2000. Petrochemical constraints for dual origin of garnet peridotites from the Dabie-Sulu UHP terrane, eastern-central China. *Journal of Metamorphic Geology*, **18,** 149–166.
Zhang, R. Y., Liou, J. G., Yang, J. S. & Ye, K., 2003. Ultrahigh-pressure metamorphism in the forbidden zone: the Xugou garnet peridotite, Sulu terrane, eastern China. *Journal of Metamorphic Geology*, **21,** 539–550.
Zhang, R. Y., Yang, J. S., Wooden, J. L., Liou, J. G. & Li, T. F., 2005a. U–Pb SHRIMP geochronology of zircon in garnet peridotite from the Sulu UHP terrane, China: implication for mantle metasomatism and subduction-zone UHP metamorphism. *Earth and Planetary Science Letter*, **237,** 729–734.
Zhang, R. Y., Liou, J. G., Zheng, J. P., Yui, Z.-F., Griffin, W. L. & O'Reilly, S. Y., 2005b. Petrogenesis of the Yangkou ultramafic complex with rhythmic layering structure from the Sulu UHP terrane, China. *American Mineralogist*, **90,** 801–813.
Zhang, R. Y., Liou, J. G., Yang, J. S. & Li, T. F., 2006a. Deep (≥200 km) continental subduction constrained by *P–T* estimates and microstructures of crust-hosted garnet peridotites. *Eos Trans AGU*, **87,** F2358.
Zhang, Z. M., Liou, J. G., Zhao, X. D. & Shi, C., 2006b. Petrogenesis of Maobei rutile eclogites from the southern Sulu ultrahigh-pressure metamorphic belt, eastern China. *Journal of Metamorphic Geology*, **24,** 727–741.
Zhang, Z., Xiao, Y., Hoefs, J., Liou, J. G. & Simon, K., 2006c. Ultrahigh pressure metamorphic rocks from the Chinese Continental Scientific Drilling Project: I. Petrology and geochemistry of the main hole (0–2,050 m). *Contributions to Mineral and Petrology*, **152,** 421–441.
Zhang, R. Y., Pan, Y. M., Yang, Y. H., Li, T. F., Liou, J. G. & Yang, J. S., 2008. Chemical composition and ultrahigh-P metamorphism of garnet peridotite from the Sulu UHP terrane, China: investigations of major, trace elements and Hf isotope of minerals. *Chemical Geology*, **255,** 250–264.
Zhang, R. Y., Liou, J. G., Zheng, J. P., Griffin, W. L., Yang, Y.-H. & Jahn, B.-M., 2009. Petrogenesis of eclogites enclosed in mantle-derived peridotites from the Sulu UHP terrane: constraints from trace elements in minerals and Hf isotopes in zircon. *Lithos*, **109,** 176–192.
Zheng, Y.-F., Zhao, Z.-F., Wu, Y.-B., Zhang, S.-B., Liu, X.-M. & Wu, F.-Y., 2006. Zircon U–Pb age, Hf and O isotope constraints on protolith origin of ultrahigh-pressure eclogite and gneiss in the Dabie orogen. *Chemical Geology*, **231,** 135–158.
Zhu, Y.-F., Massonne, H.-J. & Theye, T., 2007. Eclogite from the Chinese continental Scientific drilling borehole, their petrology and different *P–T* evolutions. *Island Arc*, **16,** 508–535.

Received 1 March 2009; revision accepted 1 June 2009.